HIGHLY LOADED COMPOSITE STRUT TEST RESULTS

K. CHAUNCEY WU and DAWN C. JEGLEY
NASA Langley Research Center, Mail Stop 190, Hampton VA 23681

ANSLEY BARNARD
Washington Space Grant Consortium, Seattle WA 98195

JAMES E. PHELPS and MARTIN J. MCKENNEY
ATK Space Systems Inc., Mail Stop 230, Hampton VA 23681

Highly loaded composite struts from a proposed truss-based Altair lunar lander descent stage concept were selected for development under NASA's Advanced Composites Technology program. Predicted compressive member forces during launch and ascent of over -100,000 lbs were much greater than the tensile loads. Therefore, compressive failure modes, including structural stability, were primary design considerations. NASA's industry partner designed and built highly loaded struts that were delivered to NASA for testing. Their design, fabricated on a washout mandrel, had a uniform-diameter composite tube with composite tapered ends. Each tapered end contained a titanium end fitting with facing conical ramps that are overlaid and overwrapped with composite materials. The highly loaded struts were loaded in both tension and compression, with ultimate failure produced in compression. Results for the two struts tested are presented and discussed, along with measured deflections, strains and observed failure mechanisms.

INTRODUCTION

NASA is interested in improving the load-carrying capability of aerospace structural components to support the goal of designing high-performance, lightweight launch vehicles and spacecraft. One example of a highly loaded truss structure is the Altair lunar lander descent stage (ref. 1), shown in Fig. 1. The lunar lander is subjected to its highest structural loads during launch from Earth, and experiences much lower mechanical loads throughout the remainder of its mission.

Since any mass landed on the moon requires several hundred times more mass to be launched from Earth, this high "gear ratio" demands that the lander structure and its components have only the minimum mass necessary to satisfy requirements (i.e., high structural efficiency). Tapered strut ends must also be considered in this application to allow large numbers of individual struts to intersect at the same node fitting. Composite materials and non-traditional manufacturing techniques offer opportunities for reducing structural mass in this application when compared to using conventional aluminum tubes with a uniform circular cross-section.

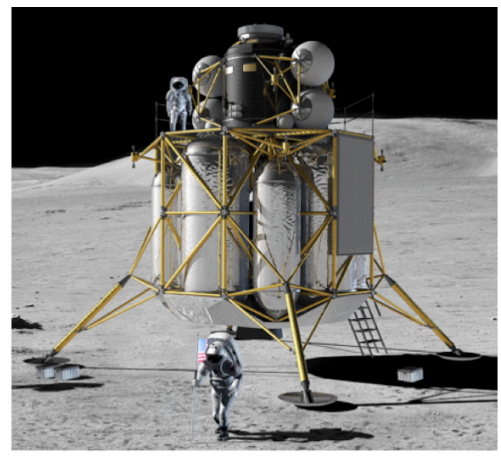

Fig. 1. Altair lunar lander concept.

The 200 struts in the lunar lander truss were arranged into 30 different groups based on their length and location in the structure.

The maximum predicted design ultimate load (DUL) experienced among these struts is -107,585 lbs in compression, and 60,182 lbs in tension. Corresponding design limit loads (DLLs) are calculated by dividing the DULs by a safety factor of 1.4.

Under NASA's Advanced Composites Technology program, a series of composite struts (ref. 2) were analyzed, designed, developed and built for Altair applications. Contractors Northrop Grumman and Boeing both designed composite struts to carry the required maximum compressive DUL, and also fabricated test articles that were evaluated by NASA under axial loading. The focus of this paper is the experimental performance of the Northrop Grumman struts (ref. 3), with selected test results described in detail in the following sections. Test results for the Boeing struts with bonded titanium end fittings (ref. 4) are presented in detail in ref. 5.

STRUT DESCRIPTION

Full-scale structural test articles were fabricated by Northrop Grumman (NG) using optimized designs developed in ref. 3. These struts were designed to support a compressive DUL of -107,585 lbs, and an axial tensile DUL of 60,182 lbs. A photograph and a sketch of a representative test article are shown in Fig. 2. Dimensions of the composite strut corresponding to the sketch are listed in Table 1.

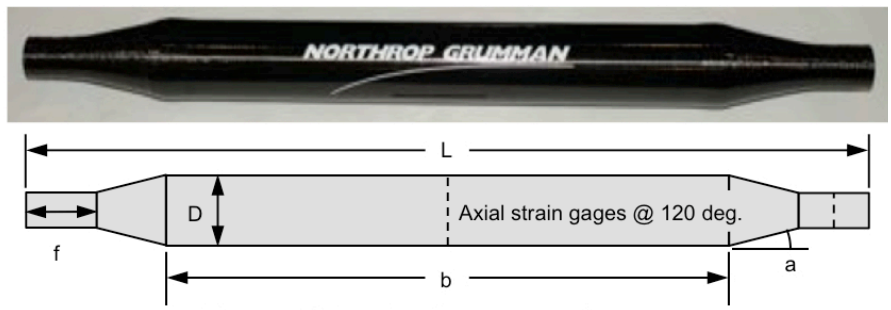

Fig. 2. Highly loaded composite strut.

Strut length L, in.	Strut body outer diam. D, in.	Strut body 0/±45/90 ply percentages	Strut body untapered length b, in.	Taper angle a, deg.	End fitting length f, in.
77.68	6.46	59/24/18	50.7	10	2.94

Table 1. Strut description.

The struts tested consisted of a carbon fiber/epoxy body fabricated using pre-impregnated (prepreg) IM7/8552 tow and tape materials. The uniform-diameter tubular composite body in the center of the strut tapered down to a smaller diameter at both ends. Titanium end fittings, shown in Fig. 3 prior to fabrication of the strut, were built into the strut ends for load introduction and to interface with the test hardware. This end fitting has several facing truncated conical ramps that are overlaid and overwrapped with the composite strut material during fabrication. The internal threads of the end fitting engage a test fitting attached to the test facility.


Fig. 3. Titanium end fitting.

To fabricate the NG struts, a washout mandrel with a cylindrical body and tapered ends was first cast from plaster in a machined mold. A central steel core inside the mandrel is used to ensure that the titanium

fittings on the strut ends are concentric with the strut axis of revolution. Additional manufacturing details for this strut are presented in ref. 3.

The cylindrical body of the NG struts had seventeen IM7/8552 plies (each 0.0052 inches thick) arranged in a $[90/0_2/\pm45/0_3/\overline{90}]_S$ stacking sequence, where the overbar indicates a shared ply across the laminate symmetry plane. Continuous prepreg tows were first wound on the mandrel to form the first 90-degree composite ply. Then, continuous 0- and ±45-degree prepreg tape plies were hand-placed on the mandrel and into the grooves of the end fittings. After winding the final 90-degree ply, additional 90-degree prepreg tows were added to the NG struts over and around the body-taper intersections (see Fig. 2) to reduce their local stress concentrations.

Finally, large numbers of 90-degree prepreg tows were wound into and around the end fitting's conical ramps, both to lock the 0- and ±45-degree plies into place, and to form a smooth outer mold line for cosmetic purposes. This approach resulted in a mechanical joint where the cured composite fibers were locked into and around the conical ramps on the end fittings. Therefore, the end fitting could not be removed from the strut if the adhesive bond with the composite failed.

STRUCTURAL ANALYSES

Classical structural analyses, performed to estimate the strut axial stiffness and Euler buckling load, are described in this section. Calculations were made assuming that the struts consist of a uniform composite tube with the maximum diameter listed in Table 1, and do not account for the tapered strut ends or end fittings. For calculation of the Euler buckling load, the tabulated strut length L was increased to account for the additional length of the test fittings used to provide pinned boundary conditions and interface with the test facility.

Assumed IM7/8552 compressive ply principal moduli E_{11} and E_{22} were 21.4 and 1.46 Mlb/in^2 (1 Mlb=10^6 lbs), respectively, with a Poisson's ratio ν_{12} of 0.34 and shear modulus G_{12} of 0.72 Mlb/in^2. Classical lamination theory was used to calculate the laminate axial modulus E of 14.11 Mlb/in^2. Using the resulting laminate thickness of 0.088 inches and a cylindrical body inner diameter of 6.28 inches, the cross-sectional area A was calculated as 1.77 in^2, and the second moment of inertia I was equal to 8.97 in^4.

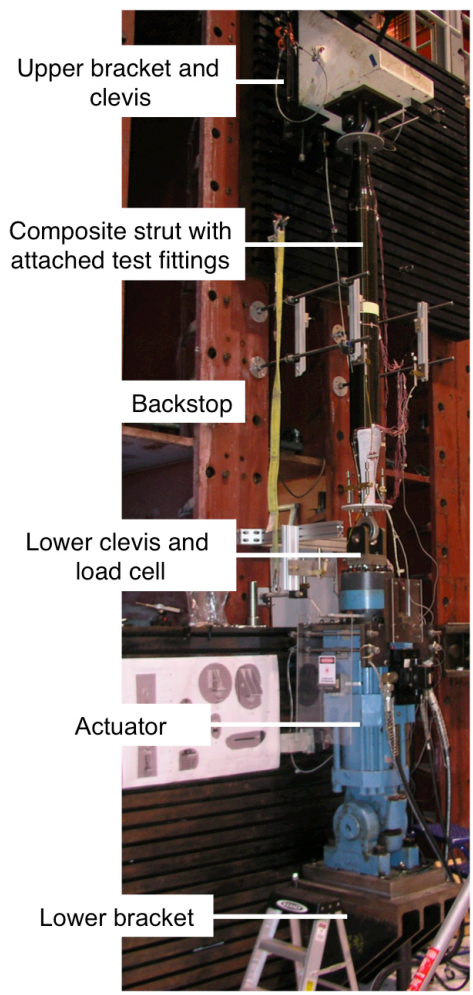

Fig. 4. Test setup.

Multiplication by the laminate axial modulus gave a predicted cross-sectional axial stiffness EA of 24.95 Mlb and bending stiffness EI of 126.53 Mlb-in^2. After division by the 77.68-inch strut length L, the predicted strut axial stiffness K=EA/L was equal to 321.2 klb/inch (1 klb=10^3 lbs). When the combined test fitting lengths of 9.5 inches were included, the overall pin center-to-pin center strut length L* was equal to L+9.5 inches, or 87.18 inches. This length was used to calculate the predicted strut Euler buckling load $P_{cr}=\pi^2EI/(L^*)^2$ of -164.3 klb.

TESTING AND INSTRUMENTATION

The struts were mounted vertically in the test fixture described in ref. 6 and loaded axially through the strut end fittings. A photograph of the test setup is shown in Fig. 4. Tang-and-clevis test fittings are threaded into the top and bottom of the strut replicate pinned end conditions, with integral spherical-bearings allowing rotation of the strut ends during load application. The upper test fitting was attached to a bracket bolted to a stiff backstop structure. The lower test fitting was attached to a 225 klb-capacity load cell, attached in series with a 225 klb-capacity actuator bolted to the backstop. Struts were loaded in displacement control using a rate of 0.001 inch/second, applied with the actuator, in either tension or compression until the desired force level or failure was reached. Each NG strut was first loaded in tension to its approximate DLL (42,987 lbs), and then to failure in compression.

The structural response of each strut was monitored during the tests using linear variable differential transformers (LVDTs), strain gages (SGs) and a digital visual image correlation (VIC) system. Instrumentation locations are shown schematically in Fig. 5, where the 0-degree orientation is normal to the backstop. Three LVDTs were mounted at 120-degree intervals around the strut circumference to measure the overall axial elongation or end shortening, and two additional LVDTs were mounted horizontally at a right angle at the strut mid-length to measure its lateral motion.

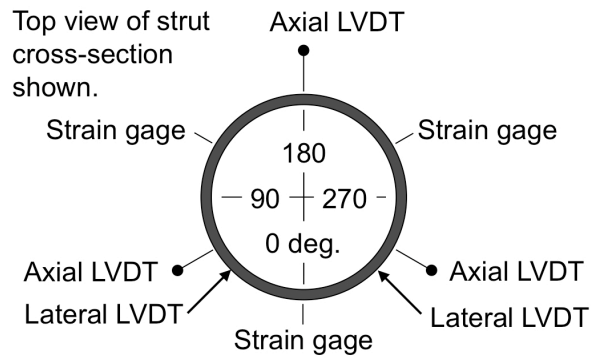

Fig. 5. Strut instrumentation layout.

Sets of three equally-spaced axial strain gages were installed around the strut outer circumference to monitor the structural response. Seven gage sets were deployed along the strut length at locations of interest, for a total of 21 axial strain gages. Additional gages were deployed around the strut mid-length to monitor the local shear and hoop strains. One end of each test specimen was painted with a speckle pattern for full-field displacement and strain monitoring over the strut taper and end fitting region using the VIC system. The strain gage and LVDT data, and VIC images of the lower region of each specimen, were all recorded at a 1 Hz rate.

RESULTS AND DISCUSSION

The measured displacements, strains and failure modes for the two highly loaded NG struts are presented and discussed in this section, and are also compared to analytical predictions. The first strut tested is denoted as NG-1, and the second strut as NG-2. Maximum tensile and compressive loads measured during the strut tests are shown in Table 2. Both of the NG struts supported tensile loads in excess of their 43.0 klb DLL, and then carried an average of 112 percent of their compressive DUL prior to failure.

Strut	Maximum tensile load, klb	Compressive failure load, klb
NG-1	44.7	-119.3
NG-2	43.8	-121.7

Table 2. Measured strut loads.

Displacements

To evaluate the NG strut structural performance, the measured tensile axial loads were first plotted versus the strut axial elongation, as shown in Fig. 6. Data for struts NG-1 and NG-2 are indicated with different colors, and the three different displacement measurements are indicated using solid and dashed lines. The average measured tensile axial stiffness of 307.9 klb/inch (calculated as the best-fit slope of the linear load versus average displacement response) for the two struts is 4.1 percent lower than the predicted axial stiffness K=EA/L of 321.2 klb/inch, which is shown in the figure as a solid gray line. The plotted responses are all very linear, with strut NG-1 having essentially no variation among the three measured displacements, and strut NG-2 showing a small variation in one of the three LVDT measurements.

The measured compressive load versus axial end shortening is shown in Fig. 7 for the two NG struts. The three separate displacement measurements for each strut are linear and agree well with each other, while diverging with increasing load. The differences noted between the individual displacements indicate that relatively small global bending occurred in the strut before failure, and are more pronounced for strut NG-2. The average measured compressive axial stiffness of 325.7 klb/inch again compares well with the analytical prediction.

The corresponding lateral deflections (measured at the strut mid-lengths) are plotted against the compressive axial loads in Fig. 8. These small measured deflections again indicate that minimal global

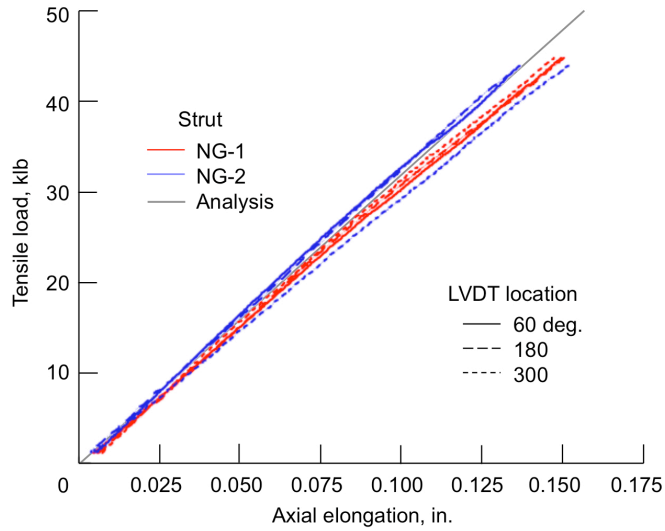

Fig. 6. Tensile load vs. axial elongation.

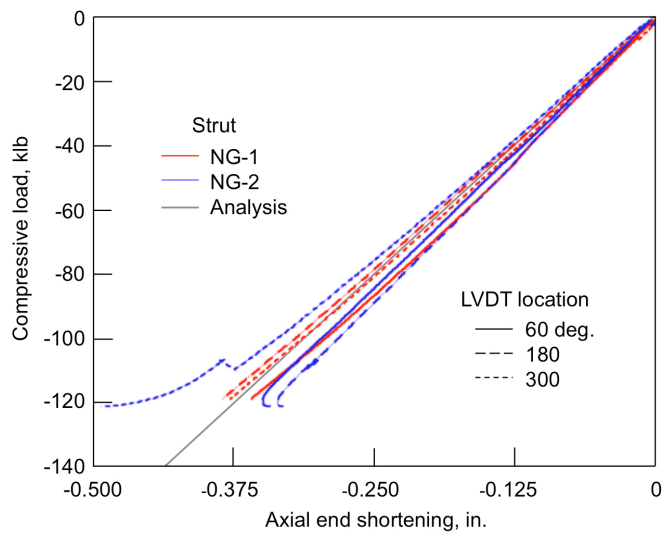

Fig. 7. Compressive load vs. axial end shortening.

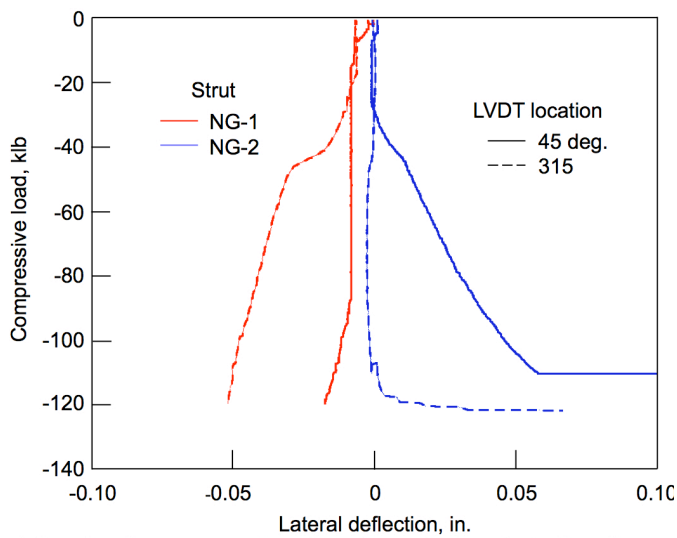

Fig. 8. Compressive load vs. lateral deflection.

bending is induced in the struts until near failure. As expected, lateral deflections for the tensile tests were very small, since the strut should not bend in tension.

Strains

Plots showing the applied tensile and compressive axial loads versus mid-length axial strains are shown in Figs. 9 and 10, respectively. Measured and predicted strains are denoted using the same colors and line styles as for the displacements. Strains for both struts are linear, and are similar between struts and around the strut circumference. However, the compressive strains for strut NG-2 diverge gradually with increasing load, and more rapidly just before global failure at -121.7 klb. The average slopes of the load versus the linear average axial strain from these plots are equal to 25.27 Mlb in tension, and 23.38 Mlb in compression. These measured values compare well to the analytical cross-sectional axial stiffness EA of 24.95 Mlb, although the average compressive stiffness is 6.3 percent lower than the predicted value.

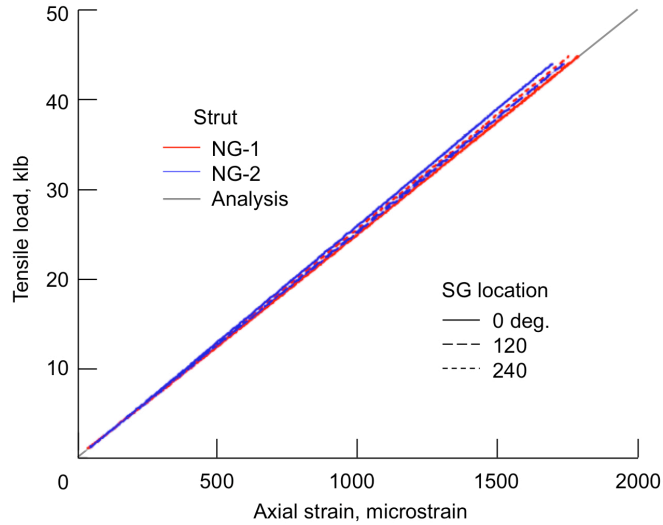

Fig. 9. Tensile load vs. mid-length axial strain.

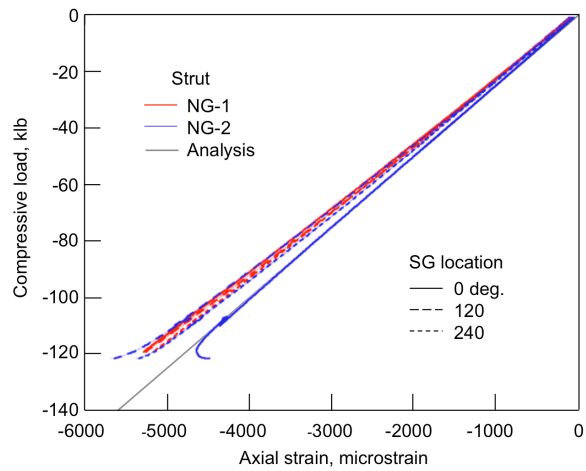

Fig. 10. Compressive load vs. mid-length axial strain.

The normalized bending strains at the NG strut mid-lengths were then calculated from the axial strains to determine their contribution to the strut compressive structural response. The bending strains shown in Fig. 10 were calculated by subtracting the average axial strain for each strut from the three individual measured axial strains. These bending strains were then normalized by dividing by the average axial strain and multiplied by 100 percent. The resulting normalized bending strains are plotted in Fig. 11. Except near the initial and final loads, the plotted normalized bending strains are small over the entire compressive load range (especially for strut NG-1), and

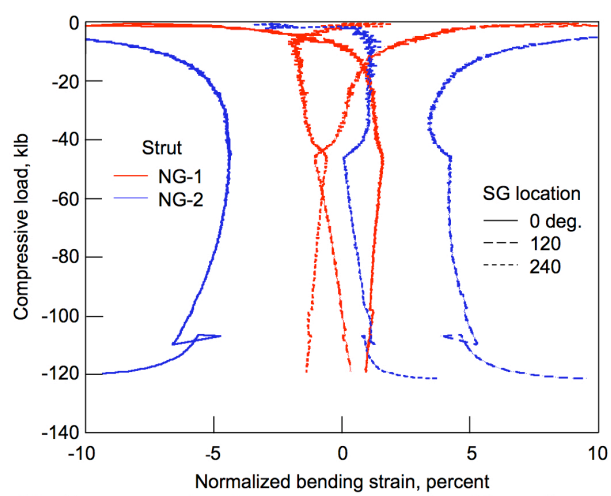

Fig. 11. Compressive load vs. normalized bending strain.

are bounded within about ±5 percent of the average axial strain, indicating that very little bending is taking place under the applied compressive loads.

Failure

During initial quasi-static axial compression of strut NG-1, several popping noises were heard around -5 klb. Loading of the strut continued with incremental application of additional axial displacement, until a sudden, large reduction in load occurred at -119.3 klb. The test was then stopped and the load removed. Except for one or two broken hoop-overwrap tows near the strut upper end, no obvious evidence of damage or failure was noted on the strut exterior. When the NG-2 strut was loaded in axial compression, an initial drop in load and noise were noted at approximately -110 klb. The axial end shortening was increased until a violent global collapse occurred at -121.7 klb.

Fig. 12. Failed strut end fitting.

In Fig. 12, the upper end of the failed NG-2 strut shows many circumferential tows overwrapped on the titanium end fitting that were destroyed when the strut failed, but no external damage was observed on the lower end of this strut. There were no non-destructive evaluations performed after testing to quantify internal damage.

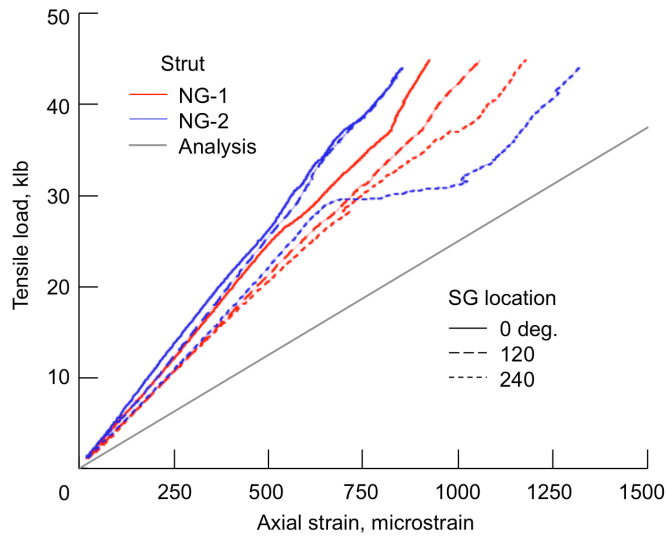

Fig. 13. Tensile load vs. upper end axial strain.

Axial strains were also measured at three points around each strut upper end fitting during the tensile and compressive tests. These data are evaluated here to provide additional insight into the structural response and failure. Axial strains, recorded at three points around the upper end fitting circumferences as shown by the dashed line in Fig. 2, are plotted against the applied tensile load for the two NG struts in Fig. 13. These axial strains are about two times lower and more nonlinear than the corresponding mid-length data in Fig. 9. This response is likely due to the large amount of material and the complex stress state in this part of the strut. The local strain discontinuity at 30 klb for strut NG-2 is believed to result from a local failure of the underlying adhesive bond between

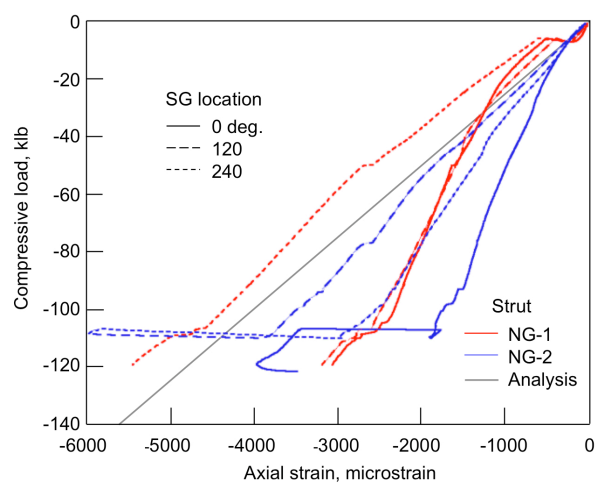

Fig. 14. Compressive load vs. upper end axial strain.

the titanium end fitting and surrounding composite structure. The compressive axial strains at the same location (shown in Fig. 14) are again lower and more nonlinear than those at the strut mid-length. The data for strut NG-1 all show a sharp jump in strains at about -5 klb, which likely corresponds to the noises noted earlier. The upper end fittings successfully carry very large compressive loads (even exceeding their DUL by over 10 percent) despite damage that may have occurred in the previous tension tests. Local failure of the upper joint of strut NG-2 is evident in the large strain discontinuities near -110 klb, and leads to the global failure at -121.7 klb.

Based on the highly localized damage observed and the minimal bending in the displacement and strain data, the failure mode for both NG struts is assessed to be material strength-driven, rather than a stiffness-based failure. This conclusion is further reinforced by the poor correlation between the measured strut failure loads (average -120.5 klb) and the predicted Euler buckling load of -164.3 klb.

CONCLUDING REMARKS

Two tapered composite struts with titanium end fittings were designed and fabricated by Northrop Grumman, and tested in axial tension and compression at the NASA Langley Research Center. Tension loads of approximately 40 klb were applied before the struts were failed in compression between -110 and -120 klb. Strength-based failures were noted in the upper end fittings of both struts. In general, the measured end-to-end deflections and mid-length axial strains were linear until the struts failed, and were well correlated with analytical predictions. Small lateral deflections and bending strains were noted throughout the tests. The struts exceeded their specified design limit load in tension, and design ultimate load in compression. Despite sustaining damage in the composite-titanium joint region, this joint concept appears to be highly robust and damage-tolerant, and may be applicable for a wide variety of structural applications.

REFERENCES

1. T.J. Collins and T. Nienaber; “Altair Lunar Lander: Design and Analysis Cycle III Structures and Mechanisms Design Summary,” presented at the NASA Johnson Space Center, Houston, TX, June 25, 2010.

2. D.C. Jegley, K.C. Wu, J.E. Phelps, M.J. McKenney and L. Oremont; “Structural Efficiency of Composite Struts for Aerospace Applications,” in Proceedings of the 52nd AIAA/ASME/ASCE/AHS/ASC Structures, Structural Dynamics and Materials Conference, Denver ,CO. April 4-7, 2011.

3. K. Pires, H. Benner, R. Deo, R. Grover, T. Palm, M. McLaughlin, E. Olason, R. Lucking and C. Collier; “Design and Manufacture of Structurally Efficient Composite Struts Concept 2: Corrugated Titanium Insert (SETS2),” Final report for NASA contract NAS NAS1-NNL04AA13B, Task NNL09AC36T, 2010.

4. R. Messinger; “Design and Manufacture of Structurally Efficient Composite Struts – Concept 1,” Final report for NASA contract NAS NAS1-NNL04AA11B, Task NNL09AC35T, 2009.

5. D.C. Jegley, K.C. Wu, J.E. Phelps, M.J. McKenney, L. Oremont and A. Barnard; “Evaluation of Long Composite Struts,” NASA/TM-2011-217049, February 2011.

6. K.C. Wu, J.E. Phelps, M.J. McKenney and D.C. Jegley; “Highly Loaded Composite Strut Test Development,“ in Proceedings of the 52nd AIAA/ASME/ASCE/AHS/ASC Structures, Structural Dynamics and Materials Conference, Denver, CO. April 4-7, 2011.